Electronic supplementary information

Interfacial Modulation of $BiVO_4$ Photoanodes with SnO_2 Quantum Dots and FeOOH for Efficient Solar-driven Water Oxidation

Kai Song [a#], Yu Hou [abc#], Lin Wang [b*], Tengfei Wang [a], Sen Cui [a],

Zhenxing Qin [a*] Zizai Ma[c*], Weiyou Yang[b], and Huilin Hou [b*]

[a] *Department of Physics, School of Applied Sciences, Taiyuan University of Science and Technology, Taiyuan, 030024, P. R. China.*

[b] *Institute of Micro/Nano Materials and Devices, Ningbo University of Technology, Ningbo 315211, P. R. China.*

[c] *College of Chemistry and Chemical Engineering, Taiyuan University of Technology, Taiyuan, 030024, China.*

[#] These authors have equally contributed to this work.

*Corresponding authors. E-mails: wanglin871014@126.com(L. Wang), qinzx@tyust.edu.cn (Z. Qin), mazizai@tyut.edu.cn (Z. Ma) and houhuilin86@163.com (H. Hou)

Tel: +86-574-87080966, Fax: +86-574-87081221.

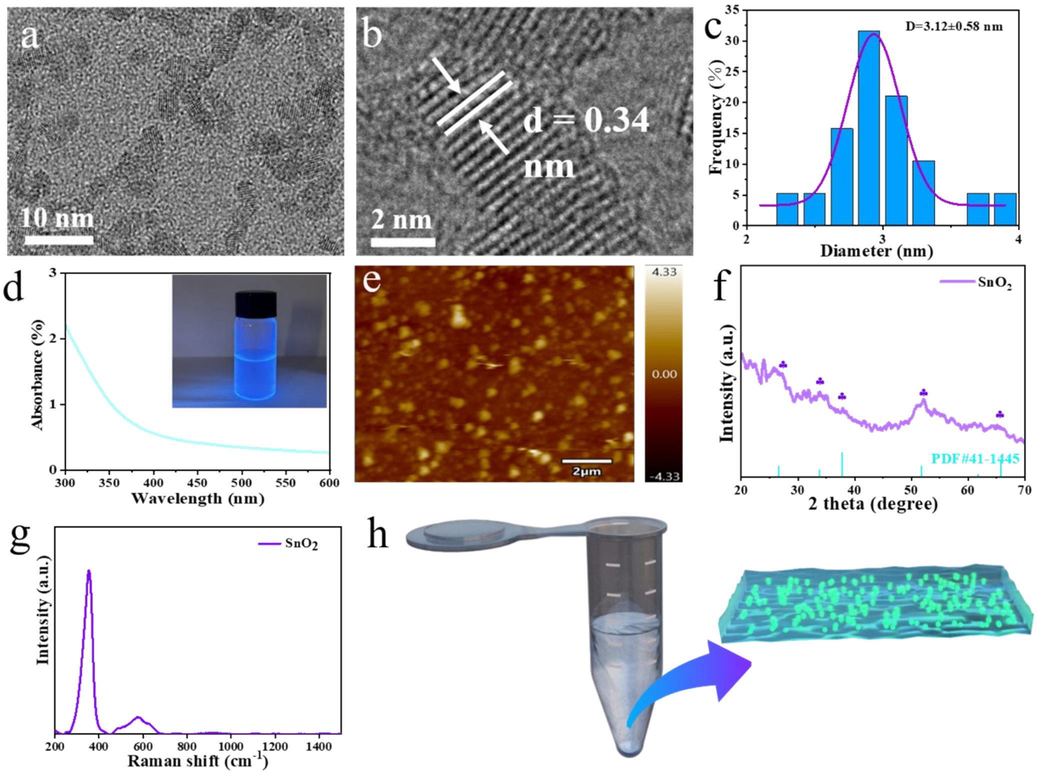

Fig. S1. (a, b) TEM images of SnO_2 QD. (c) Size histogram of SnO_2 QD. (d) UV-vis-NIR absorbance of SnO_2 QD (inset: typical Tyndall effect of SnO_2 QD, Test conditions: 2 mg SnO_2 QD dissolved in 10 ml of alcohol.). (e) AFM image of SnO_2 QD. (The unit of the brightness reference column on the right is nm) (f) XRD pattern of SnO_2 QD. (g) Raman spectrum of SnO_2 QD. (h) SnO_2 QD diagram

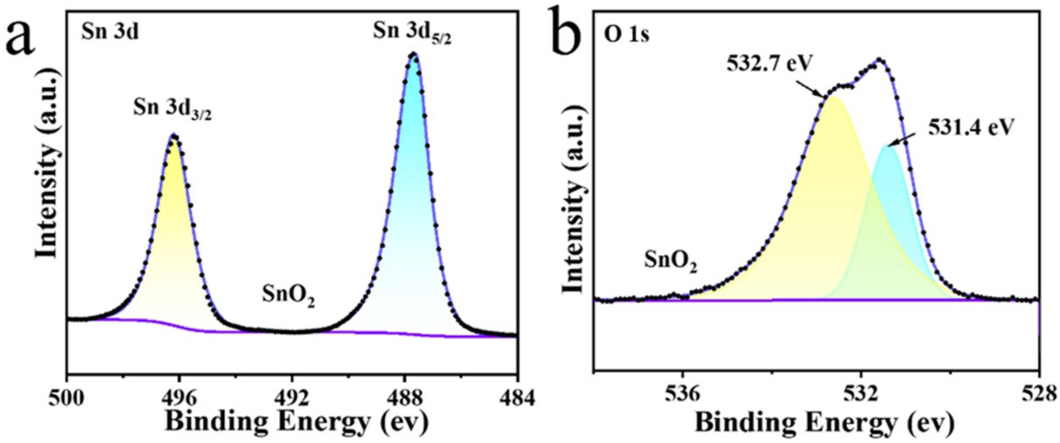

Fig. S2. (a, b) XPS spectra of the Sn 3d and O 1s binding energy regions for SnO_2 QD.

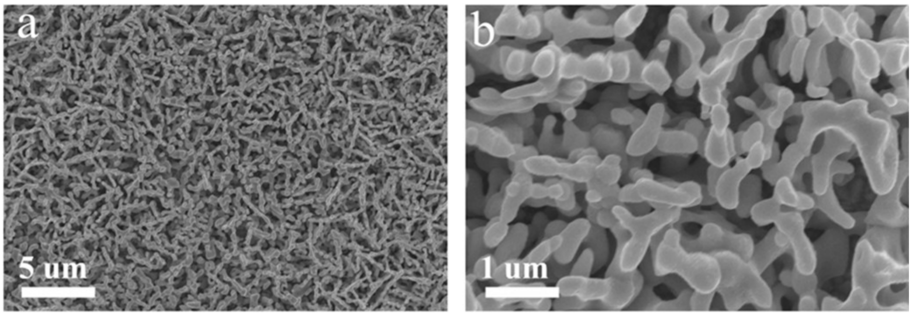

Fig. S3. (a, b) SEM images under different magnifications of our $BiVO_4$ films.

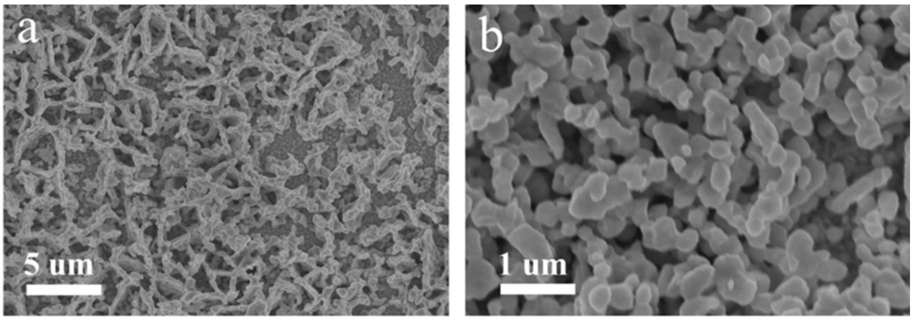

Fig. S4. (a, b) SEM images under different magnifications of our $BiVO_4$/FeOOH films.

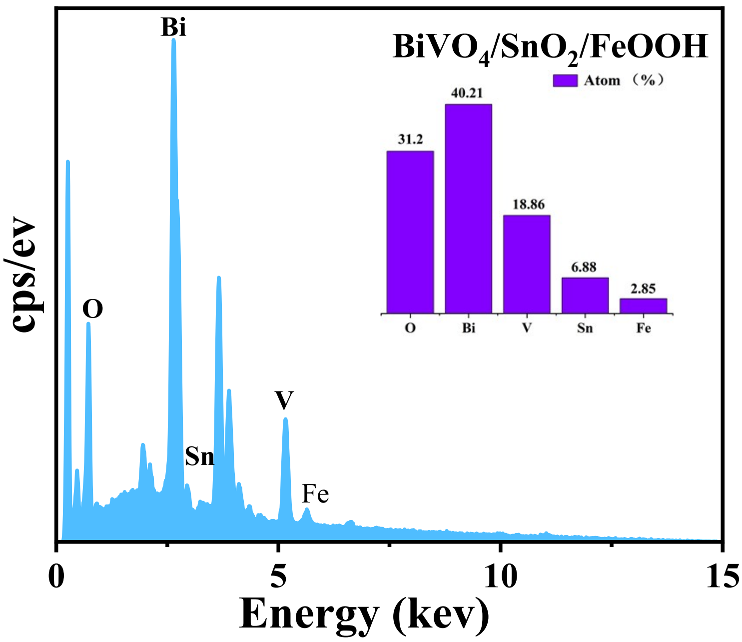

Fig. S5. EDS spectrum of $BiVO_4/SnO_2/FeOOH$ photoanodes.

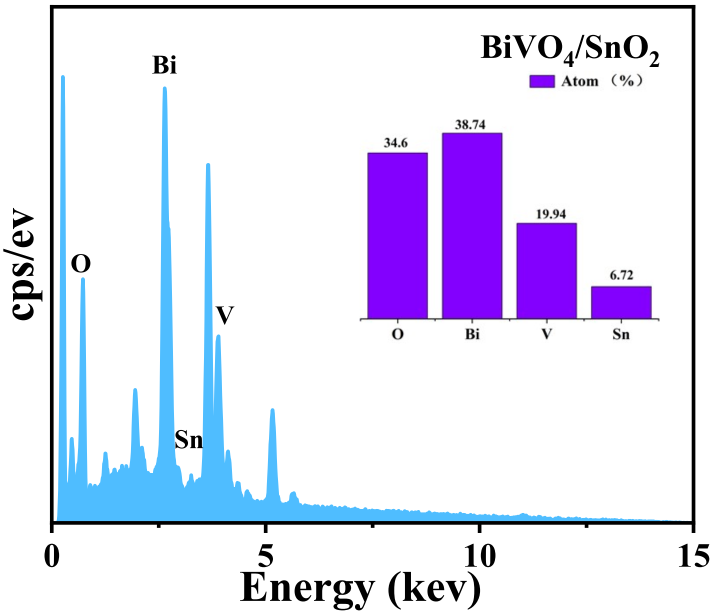

Fig. S6. EDS spectrum of $BiVO_4/SnO_2$ photoanodes.

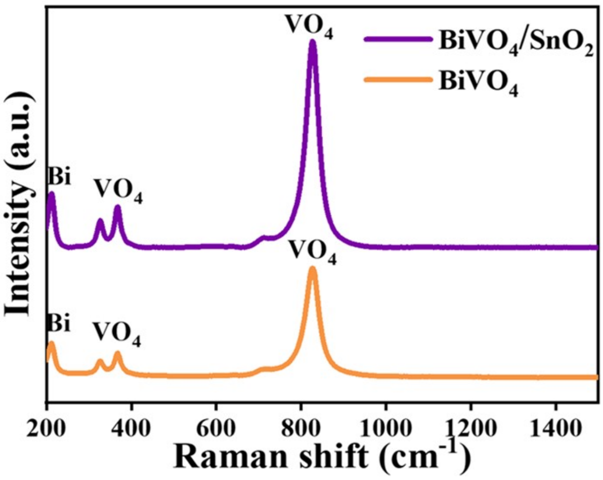

Fig. S7. Raman spectra of $BiVO_4$ and $BiVO_4/SnO_2$ photoanodes.

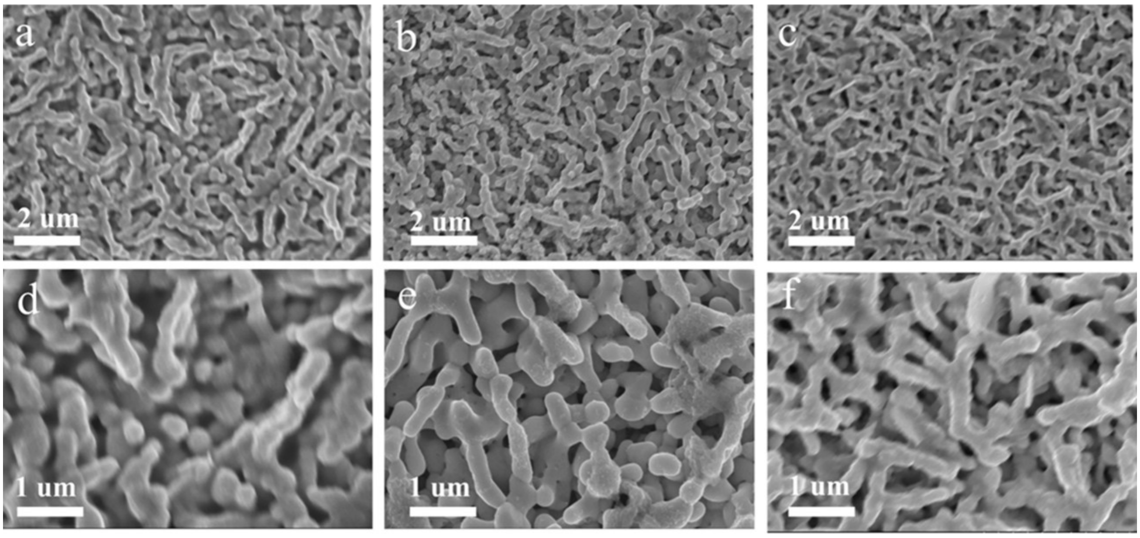

Fig. S8. SEM images under different multiples of $BiVO_4/SnO_2$ photoanode. (a-c) Low-magnification SEM images of $BiVO_4/SnO_2$ at concentrations of 0.5 mg·mL^{-1}, 1.0 mg·mL^{-1}, and 1.5 mg·mL^{-1}, respectively. (d-e) High-magnification SEM images of $BiVO_4/SnO_2$ at concentrations of 0.5 mg·mL^{-1}, 1.0 mg·mL^{-1}, and 1.5 mg·mL^{-1}, respectively.

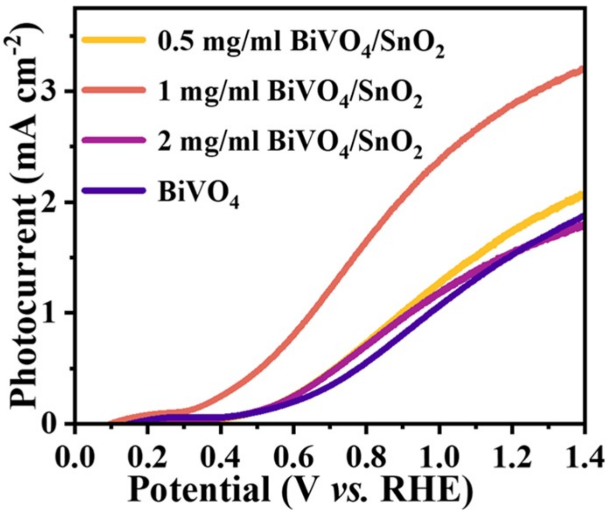

Fig. S9. LSV curves of BiVO/SnO_2 photoanodes under different concentrations (the concentration of the SnO_2 QDs solution was being altered).

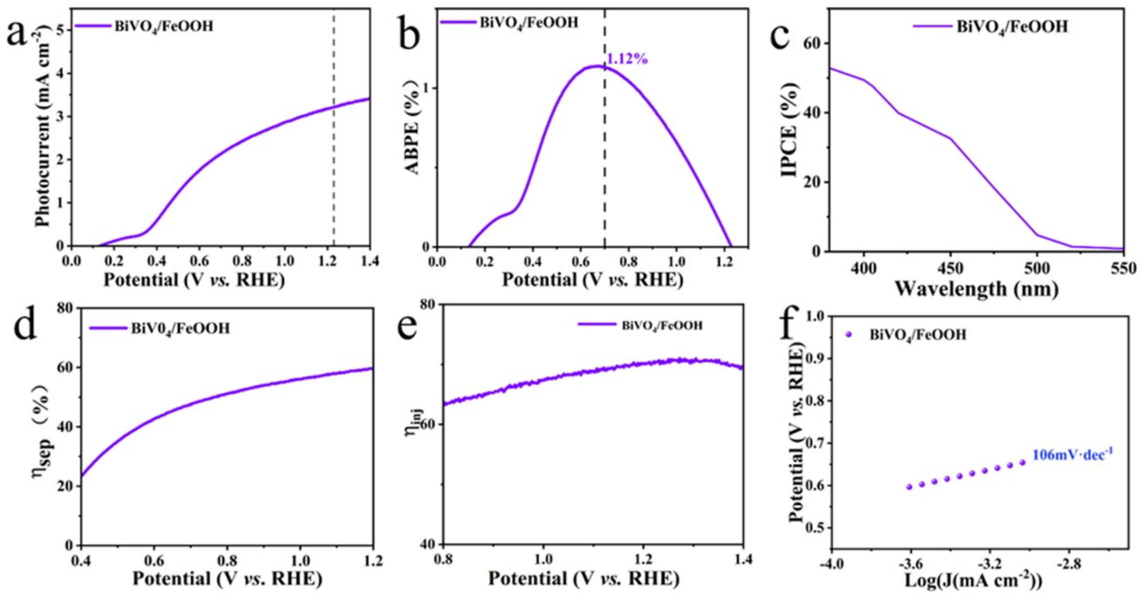

Fig. S10. (a) Linear sweep voltammogram curves. (b)ABPE curves. (c)IPCE curves. (d) Charge injection efficiency. (e) Charge separation efficiency. Measurement condition: in 0.5 M borate buffer (pH=9.5) electrolyte, AM 1.5G solar illumination. (f) Tafel plots of $BiVO_4$/FeOOH photoanode.

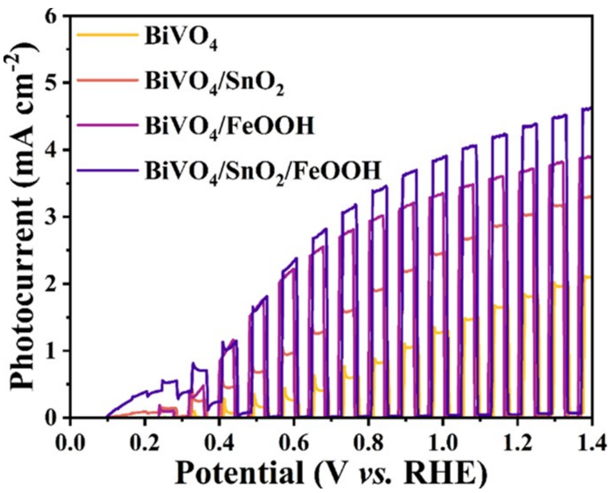

Fig. S11. Chopped J-V curve of $BiVO_4$, $BiVO_4/SnO_2$ and $BiVO_4/SnO_2/FeOOH$ photoanodes.

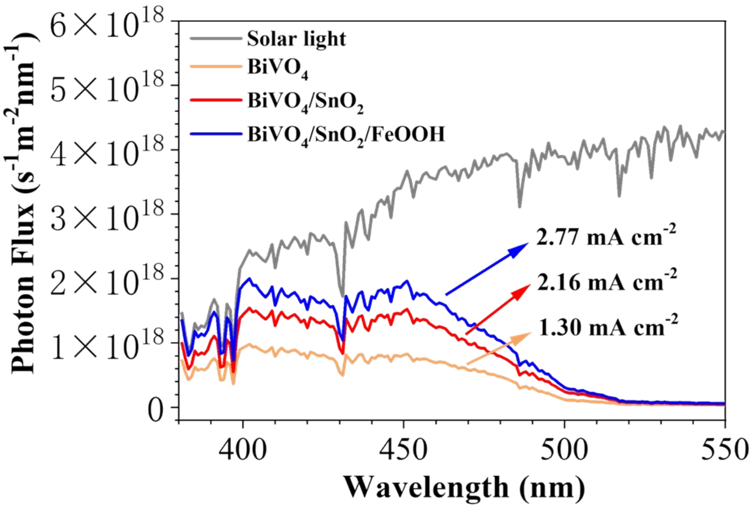

Fig. S12. Spectra of solar irradiance under AM 1.5G conditions and the modulated spectra based on the IPCE values of $BiVO_4/SnO_2$ and $BiVO_4/SnO_2/FeOOH$ photoanodes.

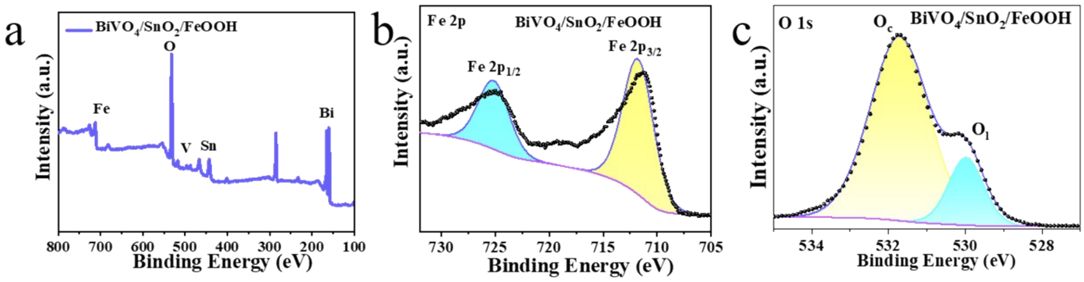

Fig. S13. (a) XPS survey spectrum, (b) Fe 2p high resolution spectrum and O 1s high resolution spectrum of $BiVO_4/SnO_2$/FeOOH photoanode after stability test.

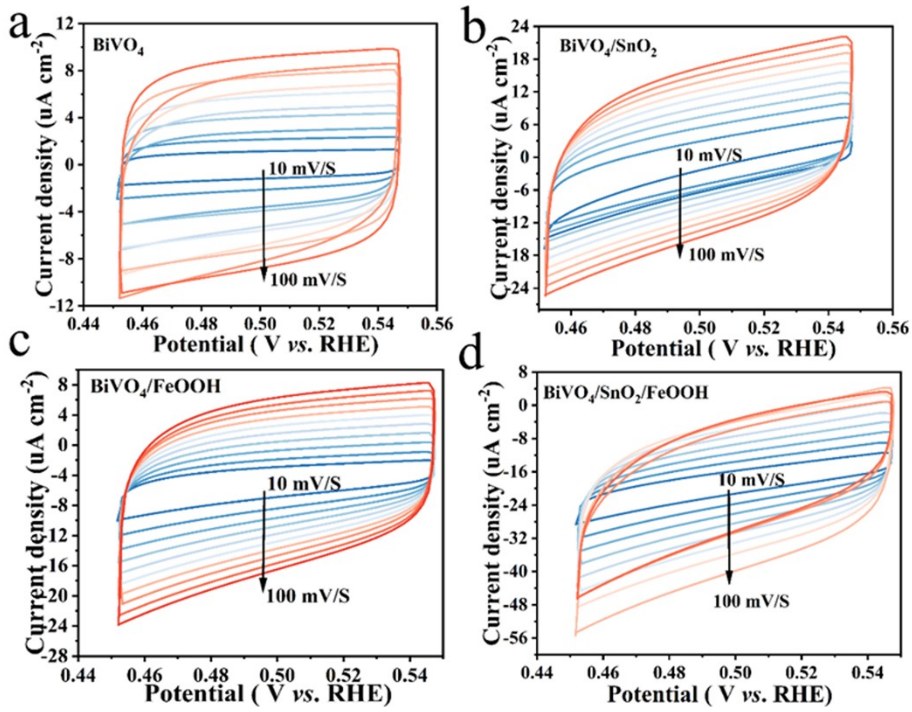

Fig. S14. CV curves of $BiVO_4$, $BiVO_4/SnO_2$ and $BiVO_4/SnO_2/FeOOH$ photoanodes with different scanning rates.

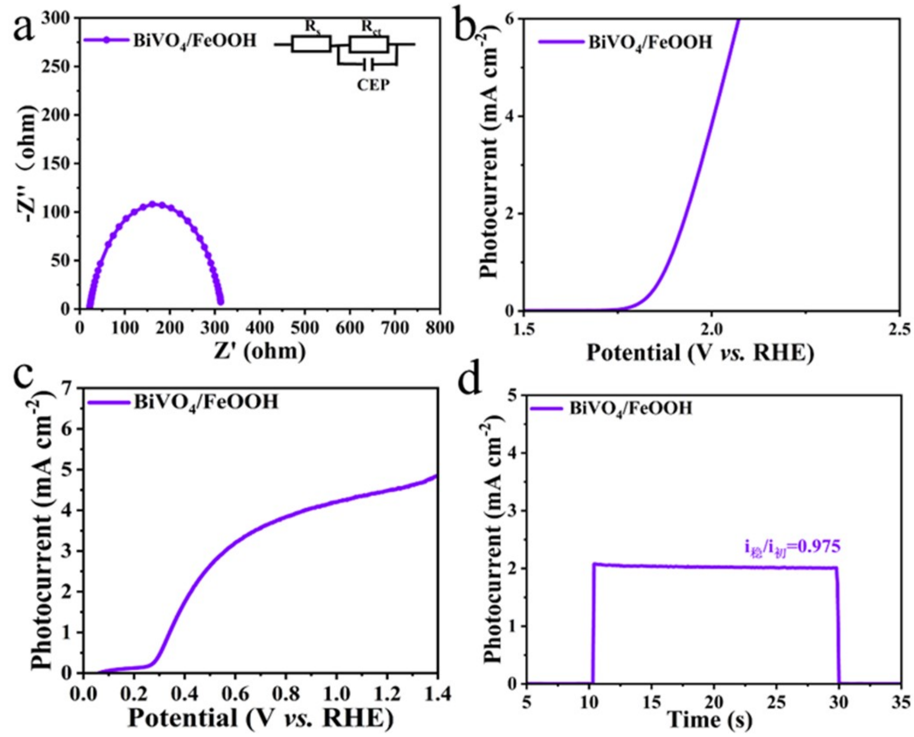

Fig. S15. (a) Nyquist plots of EIS measurements. (b) LSV curves under dark of $BiVO_4$/FeOOH photoanode. (c)The LSV curves under the presence of hole scavenger. (d)Transient photocurrent curves.

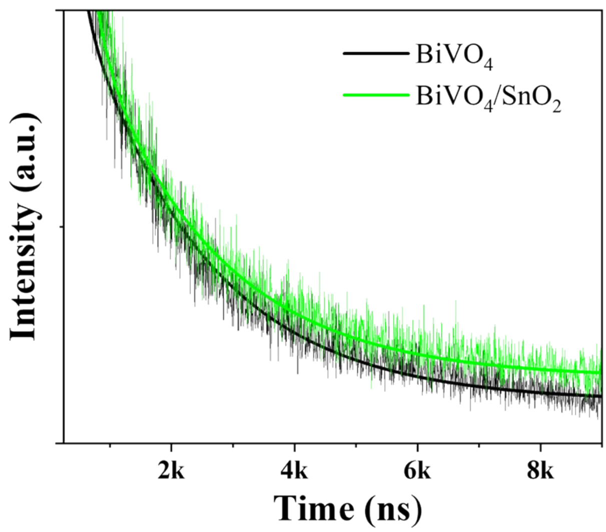

Fig. S16. TRPL spectra for $BiVO_4$ (black) and $BiVO_4/SnO_2$ (green) photoanodes.

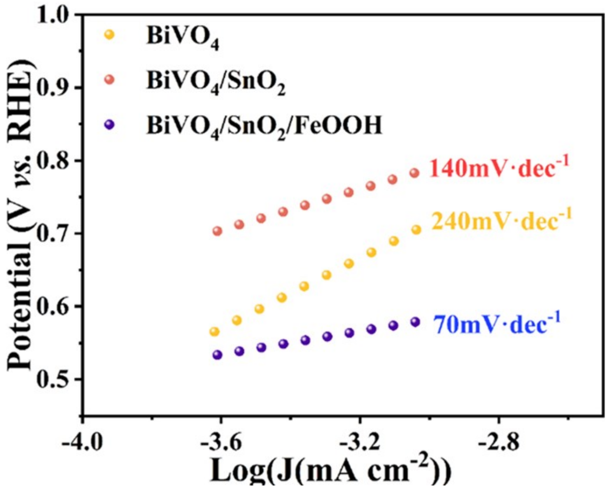

Fig. S17. Tafel plots of $BiVO_4$, $BiVO_4/SnO_2$QD and $BiVO_4/SnO_2$QD/FeOOH photoanodes.

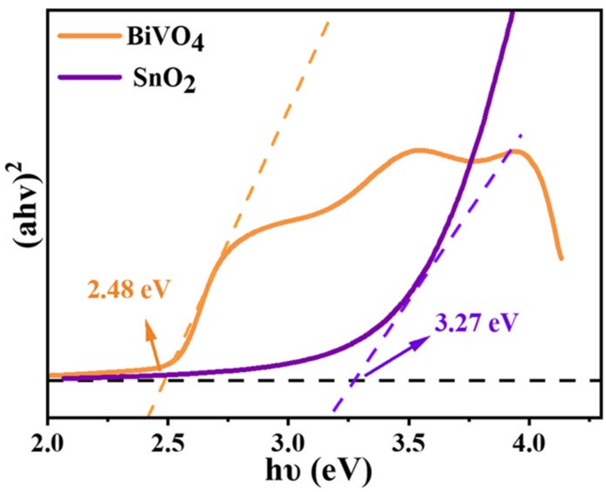

Fig. S18. Tauc plots of $BiVO_4$ and SnO_2QD.

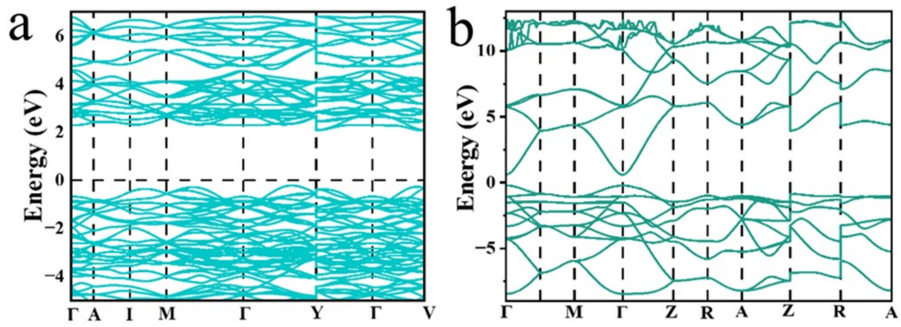

Fig. S19. (a-b) Band structures of $BiVO_4$ and SnO_2QD.

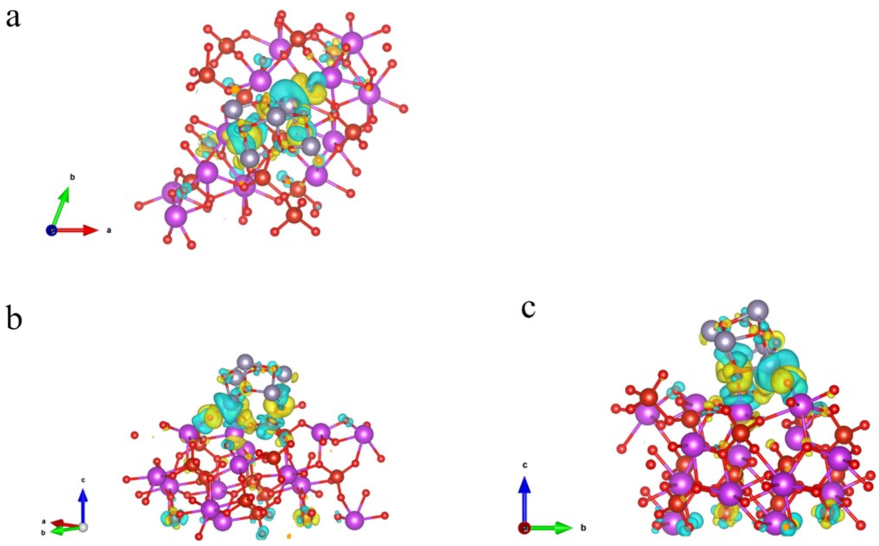

Fig. S20. (a-c) Different charge density of the $BiVO_4/SnO_2$ QD.

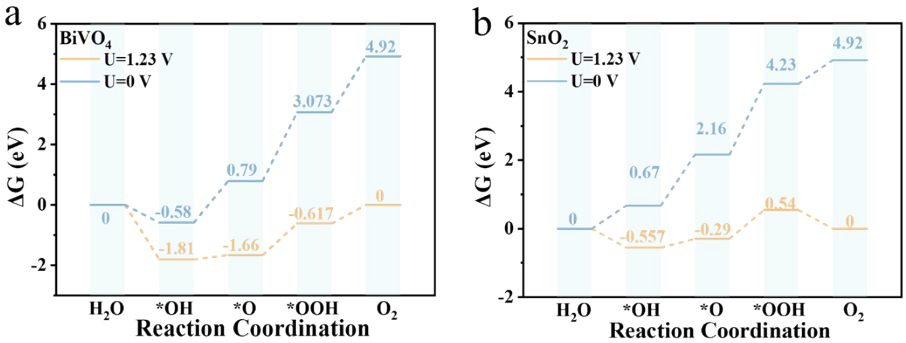

Fig. S21. (a-b) Free energy diagram (ΔG_{H2O}*) for $BiVO_4$ and SnO_2 QD.

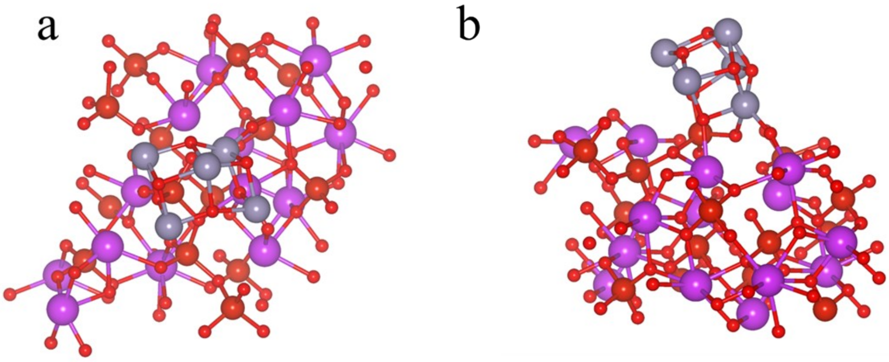

Fig. S22. Structural model diagram of $BiVO_4/SnO_2$.

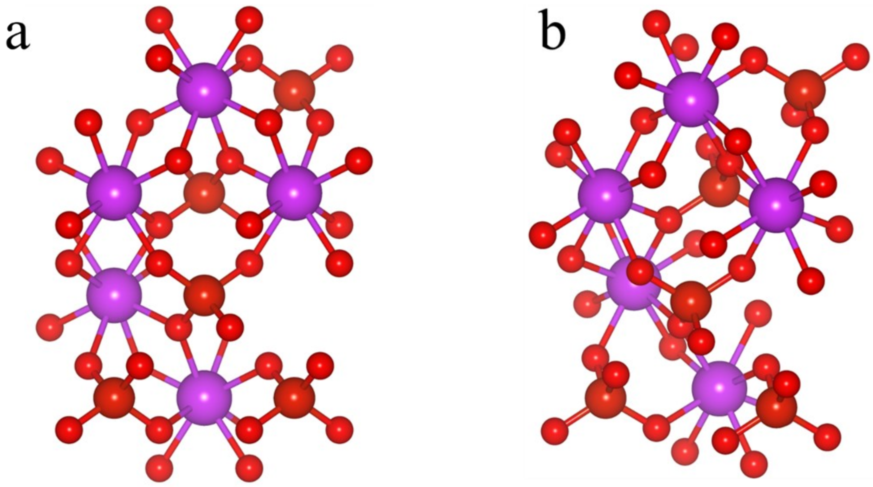

Fig. S23. Structural model diagram of $BiVO_4$.

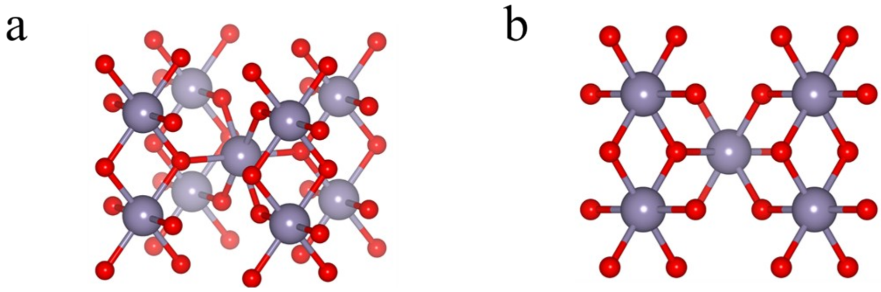

Fig. S24. Structural model diagram of SnO_2.

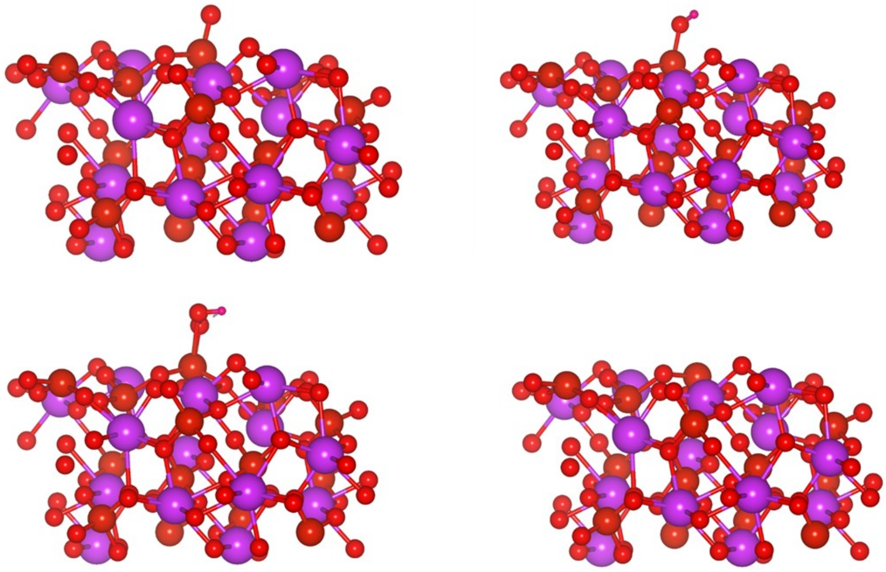

Fig. S25. Structures of the four-step oxygen evolution reaction for $BiVO_4$.

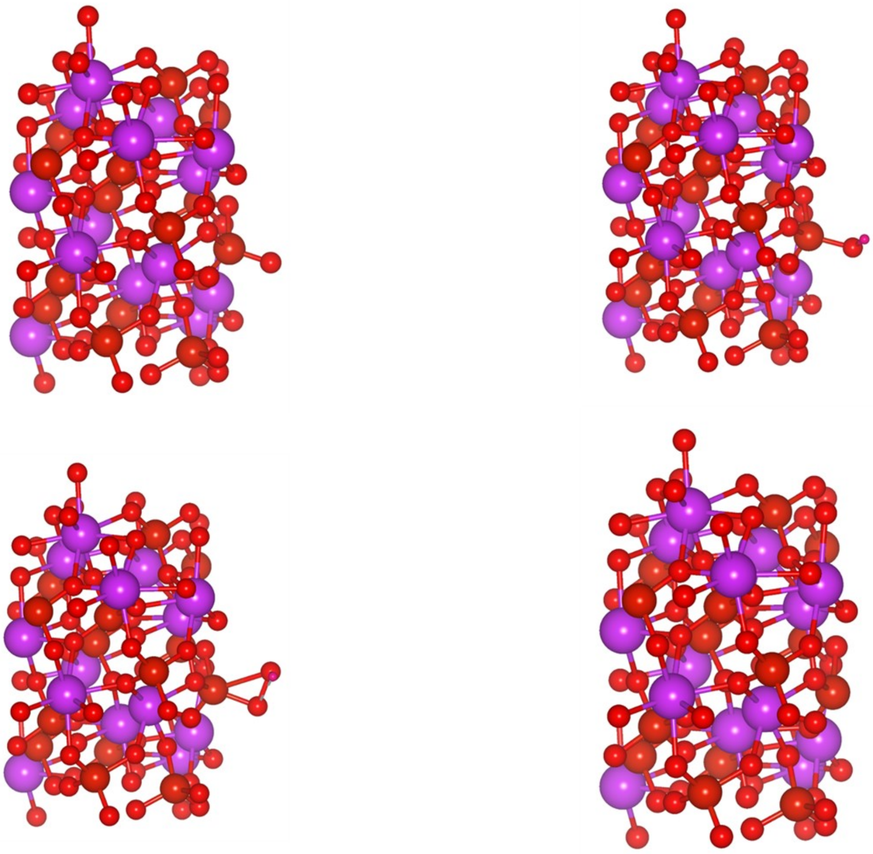

Fig. S26. Structures of the four-step oxygen evolution reaction for $BiVO_4$.

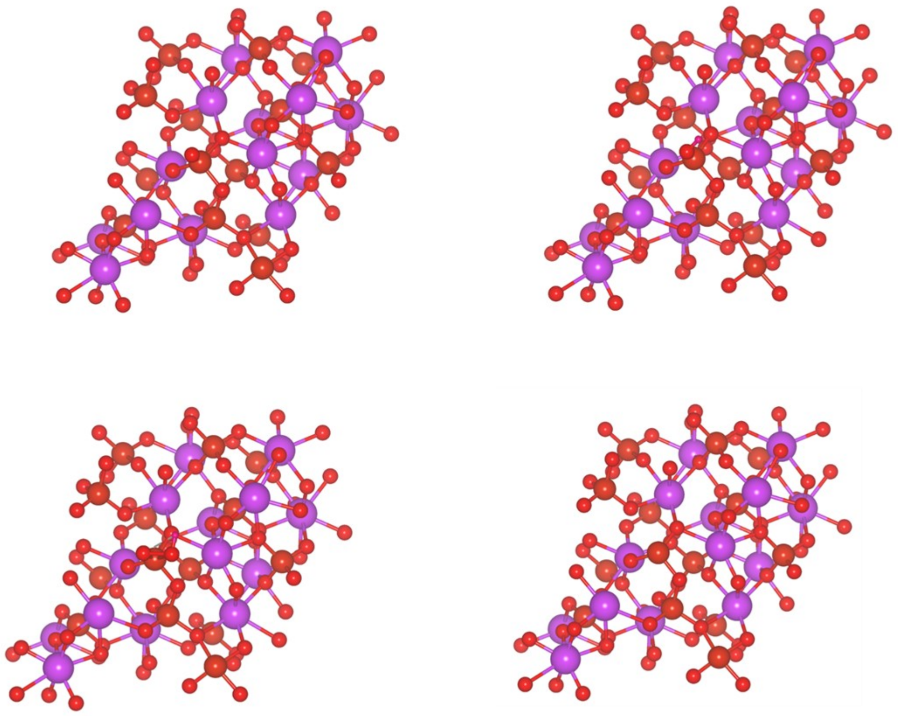

Fig. S27. Structures of the four-step oxygen evolution reaction for $BiVO_4$.

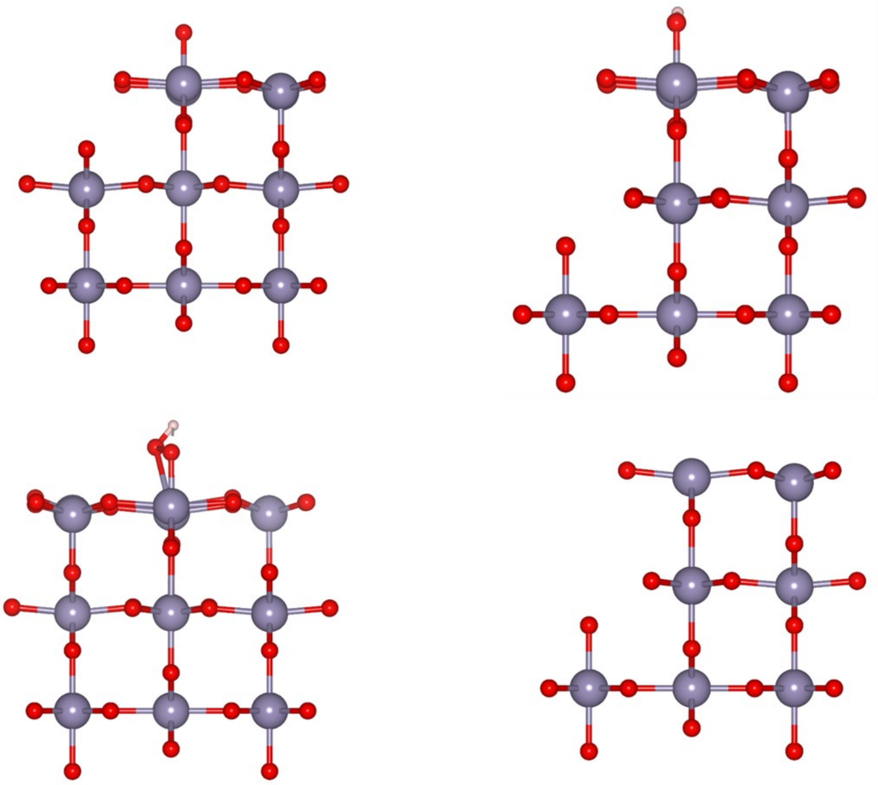

Fig. S28. Structures of the four-step oxygen evolution reaction for SnO_2.

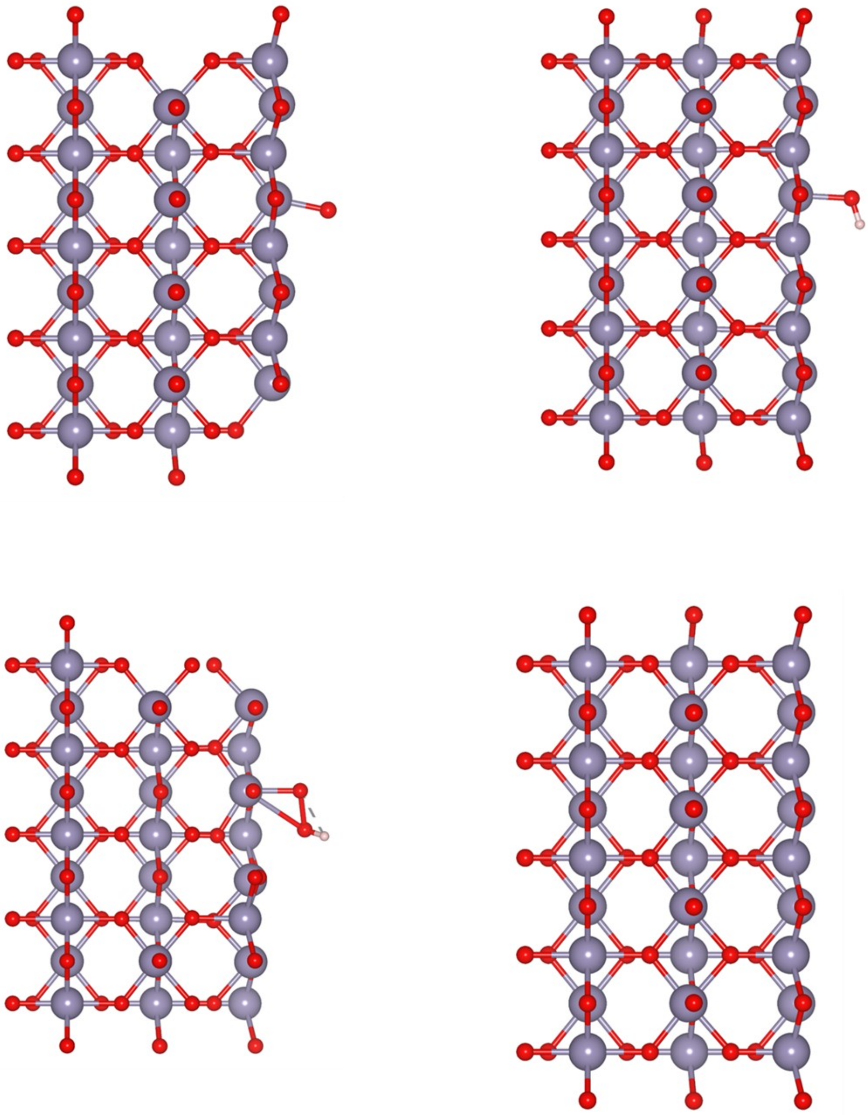

Fig. S29. Structures of the four-step oxygen evolution reaction for SnO_2.

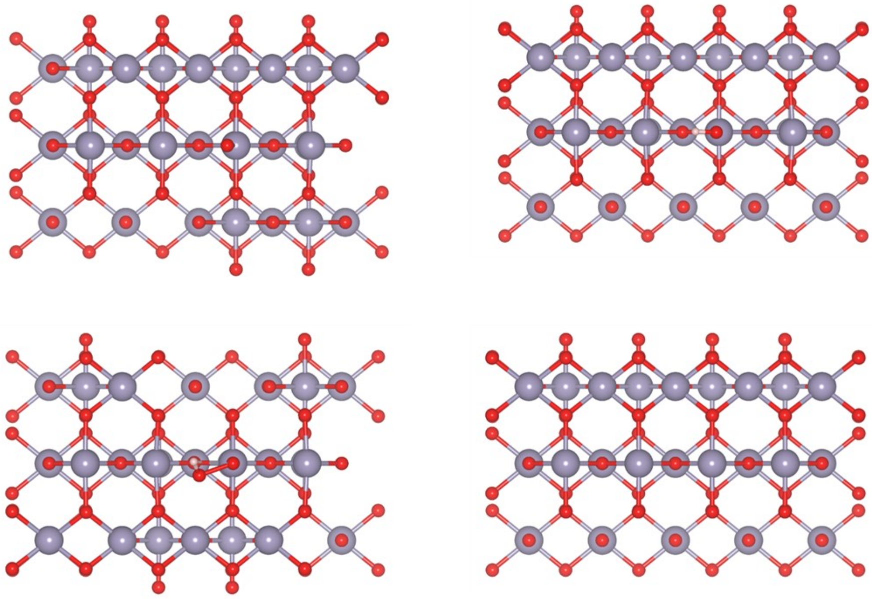

Fig. S30. Structures of the four-step oxygen evolution reaction for SnO_2.

Tab. S1 The fitted impedance values of all photoanodes**.**

Sample	$R_s(\Omega)$	$R_{ct}(\Omega)$	CPE(F)
$BiVO_4$	18.004	798.63	$3.7371*10^{-4}$
$BiVO_4/SnO_2$	22.637	247.99	$1.9737*10^{-4}$
$BiVO_4$/FeOOH	21.709	294.18	$1.3076*10^{-4}$
$BiVO_4/SnO_2$/FeOOH	19.071	232.41	$3.2641*10^{-4}$

Tab. S2. Comparison of our work with recent $BiVO_4$-based photoanodes for PEC water oxidation

Photoanode	Co-catalyst	Photocurrent density at 1.23 V_{RHE} ($mA\ cm^{-2}$)	Charge speration rate (%)	stability	Time	Ref
$BiVO_4$/CoCDS		5.26 $mA\ cm^{-2}$	86	4h	2024	1
CQDs/ $BiVO_4$	FeOOH	2.53 $mA\ cm^{-2}$	55	2h	2020	2
$BiVO_4$/SnO_2		3.76 $mA\ cm^{-2}$			2017	3
$BiVO_4$/CQDS/Ni（OH）$_2$		3.05 $mA\ cm^{-2}$	65		2023	4
CoNi-MOFs/$BiVO_4$		3.25mA cm^{-2}			2019	5
CQDs/$CdIn_2S_4$/$BiVO_4$	FeOOH	4.84 $mA\ cm^{-2}$	94.6		2022	6
BiSQD-$BiVO_4$	FeOOH	4.71 $mA\ cm^{-2}$		11h	2021	7
OV-CQDs/$BiVO_4$		4.01 $mA\ cm^{-2}$	74.3		2021	8
PbS QDs/$BiVO_4$		0.68 $mA\ cm^{-2}$			2017	9
CQDs /io-$BiVO_4$		2.25mA cm^{-2}			2015	10
QDs@LDH@BiVO4	LDH	2.23 $mA\ cm^{-2}$	50		2016	11
CeQD/$BiVO_4$	CoOx	3.98mA cm^{-2}	59	5h	2022	12

Photoanode	Co-catalyst	Photocurrent density at 1.23 V_{RHE} (mA cm^{-2})	Charge speration rate (%)	stability	Time	Ref
$BiVO_4$/NM/CQD		2.2mA cm^{-2}		24h	2024	[13]
Fe-Pi/$BiVO_4$		2.25mA cm^{-2}	63		2018	[14]
ZnOQD/$BiVO_4$		2.56mA cm^{-2}			2024	[15]
$BiVO_4$ /SnO_2 QD/FeOOH	FeOOH	3.92 mA cm^{-2}	58	24h	This work	

1. J. Lin, R. Liu, X. Li, Y. Zhao, L. Kong, Y. Li, S. Zhu and L. Wang, *Appl. Catal., B*, 2024, **343**, 123544.

2. T. S. Zhou, S. Chen, J. C. Wang, Y. Zhang, J. H. Li, J. Bai and B. X. Zhou, *Chem. Eng. J*, 2021, **403**, 126350.

3. S. Byun, B. Kim, S. Jeon and B. Shin, *J. Mater. Chem. A*, 2017, **5**, 6905-6913.

4. H. Tong, Y. Jiang and L. Xia, *Int. J. Hydrogen Energy*, 2023, **48**, 36694-36706.

5. S. Q. Zhou, K. Y. Chen, J. W. Huang, L. Wang, M. Y. Zhang, B. Bai, H. Liu and Q. Z. Wang, *Appl. Catal., B*, 2020, **266**, 118513.

6. J. Wang, T. Zhou, Y. Zhang, L. Li, C. Zhou, J. Bai, J. Li, H. Zhu and B. Zhou, *ACS Appl. Mater. Interfaces*, 2022, **14**, 45392-45402.

7. X. Y. Lu, K. H. Ye, S. Q. Zhang, J. N. Zhang, J. D. Yang, Y. C. Huang and H. B. Ji, *Chem. Eng. J.*, 2022, **428**, 131027.

8. T. Zhou, J. Wang, Y. Zhang, C. Zhou, J. Bai, J. Li and B. Zhou, *Chem. Eng. J.*, 2022, **431**, 133414.

9. L. Wang, W. Wang, W. Zhang, Y. Chen, W. Cao, H. Shi and M. Cao, *Appl. Surf. Sci.*, 2018, **427**, 553-560.

10. F. Nan, Z. Kang, J. Wang, M. Shen and L. Fang, *Appl. Phys. Lett.*, 2015, **106**, 153901.

11. Y. Tang, R. Wang, Y. Yang, D. Yan and X. Xiang, *ACS Appl. Mater. Interfaces*, 2016, **8**, 19446-19455.

12. D. H. Seo, S. Y. Hong, T. H. You, A. Sivanantham and I. S. Cho, *Chem. Eng. J.*, 2022, **450**, 137917.

13. T.-R. Kuo, Y.-T. Chiou, H.-W. Huang, C. Kongvarhodom, M. Saukani, S. Yougbaré, H.-M. Chen and L.-Y. Lin, *Int. J. Hydrogen Energy*, 2024, **51**, 1099-1108.

14. T. G. Vo, Y. Tai and C. Y. Chiang, *Appl. Catal., B*, 2019, **243**, 657-666.

15. M. R. Sui and X. Q. Gu, *J. Mater. Sci.:Mater. Electron.*, 2024, **35**, 2242.

Tab. S3 The lifetime derived from the TRPL results in Fig. S16 with double exponential fitting.

	$BiVO_4$	**$BiVO_4/SnO_2$**
τ_1/ns	226	1998
τ_2/ns	112	1983